

Kazumasa A. Takeuchi · Takuma Akimoto

# Characteristic Sign Renewals of Kardar-Parisi-Zhang Fluctuations

Received: date / Accepted: date

**Abstract** Tracking the *sign* of fluctuations governed by the  $(1+1)$ -dimensional Kardar-Parisi-Zhang (KPZ) universality class, we show, both experimentally and numerically, that its evolution has an unexpected link to a simple stochastic model called the renewal process, studied in the context of aging and ergodicity breaking. Although KPZ and the renewal process are fundamentally different in many aspects, we find remarkable agreement in some of the time correlation properties, such as the recurrence time distributions and the persistence probability, while the two systems can be different in other properties. Moreover, we find inequivalence between long-time and ensemble averages in the fraction of time occupied by a specific sign of the KPZ-class fluctuations. The distribution of its long-time average converges to nontrivial broad functions, which are found to differ significantly from that of the renewal process, but instead be characteristic of KPZ. Thus, we obtain a new type of ergodicity breaking for such systems with many-body interactions. Our analysis also detects qualitative differences in time-correlation properties of circular and flat KPZ-class interfaces, which were suggested from previous experiments and simulations but still remain theoretically unexplained.

**PACS** 89.75.Da · 05.40.-a · 02.50.-r · 64.70.qj

**Keywords** Growth phenomenon · Scaling laws · KPZ universality class · Renewal theory · Stochastic process · Weak ergodicity breaking

## 1 Introduction

The Kardar-Parisi-Zhang (KPZ) universality class [26, 2, 27, 8] is a prominent nonequilibrium class, ruling diverse kinds of nonlinear fluctuations in growing interfaces [26, 2, 46], driven particle systems [27, 8], fluctuating hydrodynamics [41], and so on. Particularly noteworthy are recent analytical developments on the  $(1+1)$ -dimensional KPZ class, which have exactly determined a number of its statistical properties on the solid mathematical basis [27, 8]. Specifically, for  $(1+1)$ -dimensional KPZ-class interfaces, the interface height  $h(x, t)$ , measured along the growth direction at lateral position  $x$  and time  $t$ , grows as

$$h(x, t) \simeq v_\infty t + (\Gamma t)^{1/3} \chi(x, t) \quad (1)$$

with parameters  $v_\infty$  and  $\Gamma$ , a rescaled random variable  $\chi$ , and  $\beta \equiv 1/3$  being the characteristic growth exponent of the  $(1+1)$ -dimensional KPZ class [26, 2]. Then the recent analytical studies [27, 8] have consistently shown that  $\chi(x, t)$  exhibits one of the few universal distribution functions, selected by the choice of the initial condition, or equivalently the global shape of the interfaces. For example, circular interfaces grown from

---

K. A. Takeuchi  
Department of Physics, Tokyo Institute of Technology, 2-12-1 Ookayama, Meguro-ku, Tokyo 152-8551, Japan.  
E-mail: kat@kaztake.org

T. Akimoto  
Department of Mechanical Engineering, Keio University, Yokohama 223-8522, Japan

a point nucleus show the largest-eigenvalue distribution of random matrices in Gaussian unitary ensemble, called the GUE Tracy-Widom distribution, while flat interfaces on a linear substrate show the equivalent for Gaussian orthogonal ensemble. This implies that the KPZ class splits into a few universality subclasses. They are also characterized by different spatial correlation functions, whose exact forms are also known analytically [27, 8]. These results for the circular and flat subclasses were corroborated by direct experimental verifications using growing interfaces of turbulent liquid crystal (LC) [47, 49, 48].

In contrast to these clear characterizations of the distribution and the spatial correlation, analytical results on the temporal correlation remain limited, hence challenging [12, 24, 13, 16]. The LC experiment [48] and numerical simulations [25, 40, 45, 7] showed that the temporal correlation is also different between the circular and flat subclasses. Firstly, the two-time correlation function <sup>1</sup>

$$\begin{aligned} C(t, t_0) &\equiv \langle h(x, t)h(x, t_0) \rangle - \langle h(x, t) \rangle \langle h(x, t_0) \rangle \\ &\simeq (\Gamma^2 t_0 t)^{1/3} C_{\text{res}}(t/t_0) \end{aligned} \quad (2)$$

was shown to decay, in its rescaled form, as  $C_{\text{res}}(t/t_0) \sim (t/t_0)^{-\bar{\lambda}}$  with  $\bar{\lambda} = 1$  for the flat case [48, 25, 7] and  $\bar{\lambda} = 1/3$  for the circular case [48, 40, 45, 7]. The latter implies  $\lim_{t \rightarrow \infty} C(t, t_0) > 0$ , i.e., correlation remains strictly positive, forever, in the circular case. Secondly, the persistence probability  $P_{\pm}(t, t_0)$  was also measured, which is defined here by the probability that the fluctuation  $\delta h(x, t) \equiv h(x, t) - \langle h(x, t) \rangle$  at a fixed position  $x$  never changes its sign (from the one denoted by the subscript) in the time interval  $[t_0, t]$ <sup>2</sup>. This quantity was found to show a power-law decay

$$P_{\pm}(t, t_0) \sim (t/t_0)^{-\theta_{\pm}^{(p)}} \quad (3)$$

with exponents  $\theta_+^{(p)} \approx 1.35 < \theta_-^{(p)} \approx 1.85$  for the flat interfaces [25, 48]<sup>3</sup> and  $\theta_+^{(p)} \approx \theta_-^{(p)} \approx 0.8$  for the circular ones [40, 48, 45]. The latter implies divergence of the mean persistence time  $\int_{t_0}^{\infty} P_{\pm}(t, t_0) dt$  in the circular case.

It has been shown that such a divergent mean leads to anomalous dynamics such as non-ergodicity, anomalous diffusion, aging, and population splitting [18, 33, 38, 39]. Therefore, the above observations on the circular KPZ subclass imply that it may also be understood in this line of research. Ergodicity is a basic concept in statistical physics and dynamical systems. It guarantees that time-averaged observables obtained by single trajectories converge to a constant (ensemble average) as time goes on. Ergodicity breaks down when, e.g., the phase space consists of mutually inaccessible regions, because then single trajectories are unable to cover the whole phase space. However, in 1992, Bouchaud [3] proposed another situation of ergodicity breaking, where the phase space is not split, but trajectories undergo long and random trapping. If the mean trapping time diverges, trajectories cannot sufficiently explore the phase space, however long they do. Interestingly, in this situation named weak ergodicity breaking (WEB) [3], certain time-averaged observables such as the time-averaged diffusion coefficient [20, 35, 1, 36, 34] and the fraction of time occupied by a given state [30, 18, 32, 33] do not converge to their ensemble average, but themselves become well-defined random variables, described by characteristic distribution functions in simple cases. The existence of such an asymptotic broad distribution for time-averaged quantities is usually regarded as a defining property of WEB. Experimentally, single-particle observations have indeed shown relevance of WEB in macromolecule diffusion in biological systems [51, 23, 50, 44, 31, 34] and in blinking quantum dots [29, 5, 43, 42]. However, it remains unclear, both theoretically and experimentally, how useful these developments on WEB are to characterize many-body problems such as the KPZ class. Therefore, it is a challenging and important issue to clarify if WEB occurs in KPZ, and if yes, characterize the WEB of the KPZ class.

<sup>1</sup> Throughout the paper,  $\langle \dots \rangle$  denotes the ensemble average defined over infinitely many realizations. It is independent of  $x$  because of the translational symmetry. Therefore, for evaluation, we can take averages over positions too to achieve better statistical accuracy, without changing its mathematical definition.

<sup>2</sup> In the literature, our definition of  $P_{\pm}(t, t_0)$  based on the ensemble average is sometimes called the ‘‘survival probability’’, in which case the term ‘‘persistence probability’’ is reserved for the probability that the sign of  $h(x, t) - h(x, t_0)$  is unchanged [4]. However, in the present paper, we define our persistence probability by the ensemble average (unless otherwise stipulated), following earlier studies of direct relevance.

<sup>3</sup>  $\theta_+^{(p)} < \theta_-^{(p)}$  holds when the underlying KPZ nonlinearity  $\frac{\lambda}{2}(\nabla h)^2$  is positive, otherwise the order is reversed [25]. Note also that the estimates obtained in [25] are somewhat different from those from the LC experiment [48]. We believe this is because of the different choice of the reference time  $t_0$ : while it was taken to be right after the initial condition in [25], times in the asymptotic KPZ regime were used in the LC experiment [48]. This is also the choice of the present paper; therefore, here we refer to the estimates from the LC experiment,  $\theta_+^{(p)} \approx 1.35$  and  $\theta_-^{(p)} \approx 1.85$ , as the values of the persistence exponents for the flat KPZ subclass.

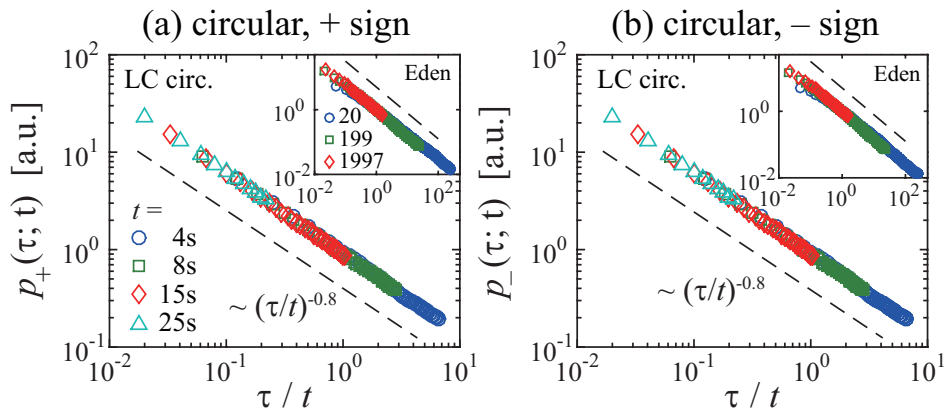


**Fig. 1** Waiting-time distributions (ccdfs)  $p_{\pm}(\tau;t)$  against  $\tau/t$  for the circular interfaces, obtained at different  $t$  in the LC experiment (main panels) and the Eden model (insets). The dashed lines are guides to the eyes indicating exponent  $-0.8$ . The same set of colors/symbols and  $t$  is used in both panels. The ordinates are arbitrarily shifted.

## 2 Our approach

To investigate possible relationship between WEB and KPZ, we construct a dichotomous process from height fluctuations of KPZ-class interfaces,  $\sigma(x,t) \equiv \text{sign}[\delta h(x,t)]$ , which is then regarded as a time series. Such dichotomization has recently been used to characterize time-correlation properties of interactions on lipid membranes [52,53] and of turbulence [22,21], successfully. The constructed process is compared with a theoretically defined dichotomous process, arguably the simplest and best-studied one, namely the renewal process (RP) [15,9,18]. RP consists of a single two-state variable, which switches from one to the other state after random, uncorrelated waiting times generated by a power-law distribution:

$$p(\tau) \equiv \text{Prob}[\text{waiting time} > \tau] = \left(\frac{\tau}{\tau_0}\right)^{-\theta}, \quad (\tau \geq \tau_0). \quad (4)$$

This model shows WEB and aging for  $0 < \theta < 1$  [15,9,18,39].

Concerning KPZ-class interfaces, we use the experimental data of the circular and flat interfaces obtained in Refs. [49,48] (LC turbulence): for the circular (or flat) case, total observation time was  $T_{\text{tot}} = 30.5\text{s}$  (63s), time resolution was  $T_{\text{res}} = 0.5\text{s}$  (0.35s), and  $N = 955$  (1128) realizations were used, respectively. We also analyze newly obtained numerical data for circular interfaces of the off-lattice Eden model [45] ( $T_{\text{tot}} = 5000$ ,  $T_{\text{res}} = 1$ ,  $N = 5000$ ) and flat interfaces of the discrete polynuclear growth (dPNG) model ( $T_{\text{tot}} = 10^4$ ,  $T_{\text{res}} = 0.1$ ,  $N = 10^4$ ). Further descriptions of the systems and parameters are given in Appendix A.

## 3 Results

### 3.1 Circular interfaces

First of all, we stress that RP is far too simple to fully describe KPZ, because RP is a two-state model without even spatial degrees of freedom and has uncorrelated waiting times. We nonetheless measure the waiting times between two sign changes of  $\delta h$ , first for the circular interfaces, for which we anticipate relation to WEB as discussed above. More specifically, we define the waiting-time distribution  $p_{\pm}(\tau;t)$  by the probability that the sign renewed at time  $t$  (changed to the subscripted one) lasts over time length  $\tau$  or longer, hence  $p_{\pm}(\tau;t)$  is the complementary cumulative distribution function (ccdf). Figure 1 shows the results for both the LC experiment (main panels) and the Eden model (insets). Remarkably, in both cases we find a clear power law as described in Eq. (4) with exponent  $\theta = 0.8$ , while the cutoff  $\tau_0$  is out of the range of our resolution.

This similarity to RP leads us to compare further statistical properties between the two systems. First we focus on the forward recurrence time  $\tau_f(t)$ , defined as the interval between time  $t$  and the next sign change, as well as the backward recurrence time  $\tau_b(t)$ , which is the backward interval from  $t$  to the previous sign change

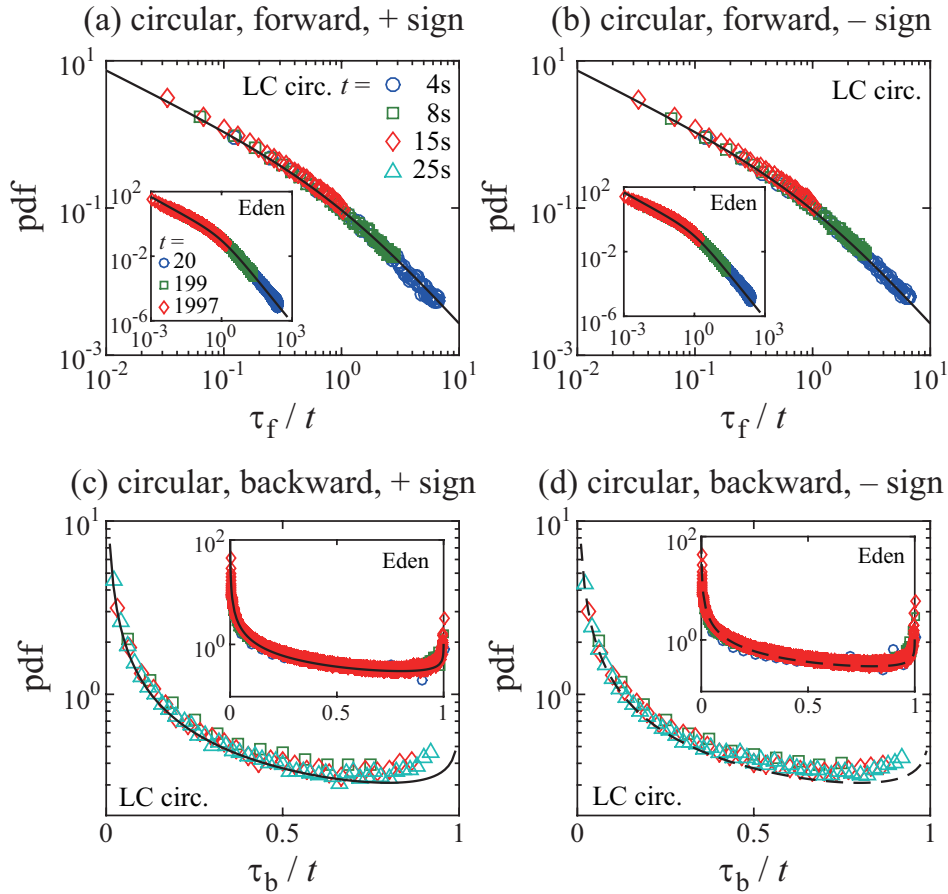


**Fig. 2** Distributions (pdfs) of the forward (a,b) and backward (c,d) recurrence times,  $\tau_f$  and  $\tau_b$ , respectively, for the circular interfaces at different  $t$  in the LC experiment (main panels) and the Eden model (insets).  $\tau_f$  and  $\tau_b$  are rescaled by  $t$ . The black lines indicate RP's exact results, Eqs. (5) and (6), with  $\theta = 0.8$ . The data are normalized so that they have the same statistical weight as RP's exact results in the range covered by their abscissa. The same set of colors/symbols and  $t$  is used in all panels. Note that data at  $t = 25$  s are not shown for  $\tau_f$  because the remaining time is then too short to measure the distribution of  $\tau_f$ .

[18, 14, 15]. For RP, Dynkin [14, 18] derived exact forms of the probability density function (pdf) of  $\tau_f(t)$  and  $\tau_b(t)$  as follows, for  $0 < \theta < 1$ :

$$\text{pdf}(\tilde{\tau}_f) = \frac{\sin \pi \theta}{\pi} \frac{1}{\tilde{\tau}_f^\theta (1 + \tilde{\tau}_f)}, \quad (5)$$

$$\text{pdf}(\tilde{\tau}_b) = \beta_{1-\theta, \theta}(\tilde{\tau}_b) \equiv \frac{\sin \pi \theta}{\pi} \tilde{\tau}_b^{-\theta} (1 - \tilde{\tau}_b)^{\theta-1}, \quad (6)$$

with  $\tilde{\tau}_f \equiv \tau_f/t$ ,  $\tilde{\tau}_b \equiv \tau_b/t$  and  $\beta_{a,b}(x)$  denoting the pdf of the beta distribution. Although their derivation essentially relies on the independence of waiting times in RP, a feature not shared with KPZ, we find, as shown in Fig. 2, that both experimental and numerical results for the circular interfaces precisely follow RP's exact results indicated by the solid lines (except finite-time corrections). Note that the persistence probability  $P_\pm(t, t_0)$  considered in Eq. (3) actually amounts to the ccdf of  $\tau_f(t_0)$ , i.e.,  $P_\pm(t, t_0) = \int_{t-t_0}^\infty \text{pdf}(\tau_f(t_0)) d\tau_f$ . This indicates that the functional form of the persistence probability, which is usually intractable for such spatially-extended nonlinear systems [4], seems to be given by RP's exact result (5) in the case of the circular KPZ subclass. We also remark that the explicit dependence of the pdfs on  $t$  indicates the aging of the system.

In contrast to this agreement, we also find statistical properties that are clearly different between the two systems. The occupation time  $T_+$ , i.e., the length of time spent by the positive sign, is a quantity well-studied in two-state stochastic processes [30, 18] and in more general scale-invariant phenomena (see, e.g., [11]). It is simply related to the time-averaged sign  $\bar{\sigma} \equiv (1/T) \int_0^T \sigma(x, t) dt$  by  $\bar{\sigma} = 2T_+/T - 1$ . For RP with  $0 < \theta < 1$ ,

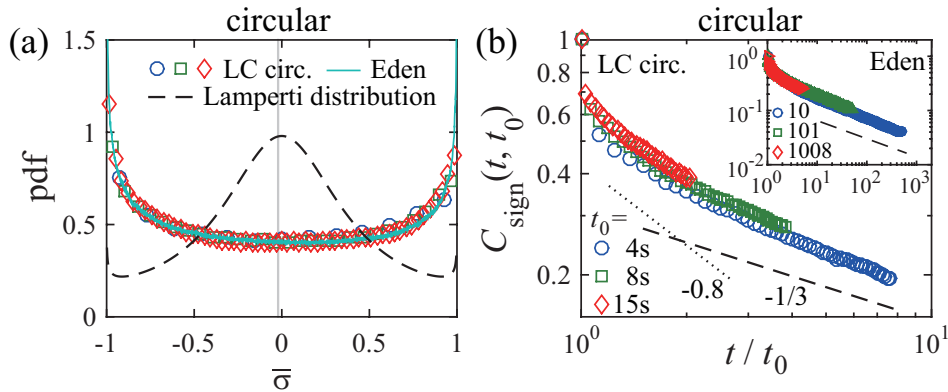


**Fig. 3** Time-averaged sign distribution (a) and sign correlation function (b) for the circular interfaces. (a) Pdf of the time-averaged sign  $\bar{\sigma} = (1/T) \int_0^T \sigma(x, t) dt$  for the LC experiment ( $T = 7.5$  s, 15 s, 30.5 s for circles, squares, and diamonds, respectively) and the Eden model ( $T = 5000$ ), compared to the Lamperti distribution (7) with  $\theta = 0.8$  (dashed line). The gray vertical line indicates the ensemble-averaged value  $\langle \sigma \rangle = -0.021$ . The existence of the broad asymptotic distribution is a direct evidence of WEB in the circular KPZ subclass. (b) Correlation function of sign,  $C_{\text{sign}}(t, t_0) = \langle \sigma(x, t) \sigma(x, t_0) \rangle$ , measured at different  $t_0$  for the LC experiment (main panel) and the Eden model (inset). The dashed and dotted lines indicate exponents  $-\bar{\lambda} = -1/3$  and  $-\theta = -0.8$ , respectively.

Lamperti [30] showed that it does not converge to the ensemble average, but remains stochastic even for  $T \rightarrow \infty$ , with its pdf derived exactly as follows [30, 18]:

$$\text{pdf}(\bar{\sigma}) = \frac{(2 \sin \pi \theta / \pi) (1 - \bar{\sigma}^2)^{\theta-1}}{(1 + \bar{\sigma})^{2\theta} + (1 - \bar{\sigma})^{2\theta} + 2(\cos \pi \theta) (1 - \bar{\sigma}^2)^\theta}. \quad (7)$$

This distributional behavior of the time-averaged sign is a clear evidence of WEB in RP. The corresponding pdfs obtained at different  $T$  for the circular KPZ interfaces [Fig. 3(a) symbols] indeed indicate an asymptotic broad distribution, demonstrating that  $\bar{\sigma}$  remains stochastic and does not converge to the ensemble average  $\langle \sigma \rangle = -0.021$  (determined by the GUE Tracy-Widom distribution) shown by the gray vertical line in Fig. 3(a). This demonstrates that KPZ indeed exhibits WEB, at least for the circular case. On the other hand, the found distribution is clearly different from the Lamperti's one for RP with  $\theta = 0.8$  (black dashed line). We find instead a nontrivial distribution universal within the circular KPZ subclass, as supported by good agreement between experiments and simulations (symbols and turquoise solid line).

Another quantity of interest is the correlation function of sign,  $C_{\text{sign}}(t, t_0) \equiv \langle \sigma(x, t) \sigma(x, t_0) \rangle$ . This can be expanded by the generalized persistence probability  $P_{\pm, n}(t, t_0)$ , i.e., the probability that the sign changes  $n$  times between  $t_0$  and  $t$  (hence  $P_{\pm, 0}(t, t_0) = P_{\pm}(t, t_0)$ ):

$$C_{\text{sign}}(t, t_0) = \sum_{\pm} P_{\pm}(t_0) \sum_{n=0}^{\infty} (-1)^n P_{\pm, n}(t, t_0), \quad (8)$$

where  $P_{\pm}(t_0)$  denotes the probability that fluctuations at  $t_0$  take the sign indicated by the subscript. For RP with  $0 < \theta < 1$ , one can explicitly calculate the infinite sum of Eq. (8) and obtain  $C_{\text{sign}}(t, t_0) \simeq \sum_{\pm} P_{\pm}(t_0) P_{\pm, 0}(t, t_0) \sim (t/t_0)^{-\theta}$  [18]. In contrast, for the circular KPZ interfaces, we find that  $C_{\text{sign}}(t, t_0)$  decays as  $C_{\text{sign}}(t, t_0) \sim t^{-\bar{\lambda}}$  with  $\bar{\lambda} = 1/3$  [Fig. 3(b)] (see also footnote 4), in the same way as the rescaled correlation function  $C_{\text{res}}(t/t_0)$  does [Eq. (2)]. Since the relation (8) holds generally and  $P_{\pm, 0}(t, t_0) = \int_{t-t_0}^{\infty} \text{pdf}(\tau_f(t_0)) d\tau_f$  is alike, the difference from RP should stem from  $P_{\pm, n \geq 1}(t, t_0)$ , which encodes correlation between waiting times. For RP, one can show

$$P_{\pm, n \geq 1}(t_0 + \Delta t, t_0) \sim \begin{cases} \Delta t^{-2\theta+1} & \text{for } \Delta t \ll t_0, \\ \Delta t^{-\theta} & \text{for } \Delta t \gg t_0, \end{cases} \quad (9)$$

with  $t_0, \Delta t \gg \tau_0$  (see Appendix B). Now, for the circular KPZ interfaces, the results in Fig. 4 show that the long-time behavior seems to be consistent with that of RP<sup>4</sup>, but the short-time behavior for odd  $n$  shows faster

<sup>4</sup> For some quantities the asymptotic decay is only reached by the numerical data, obtained with longer time.

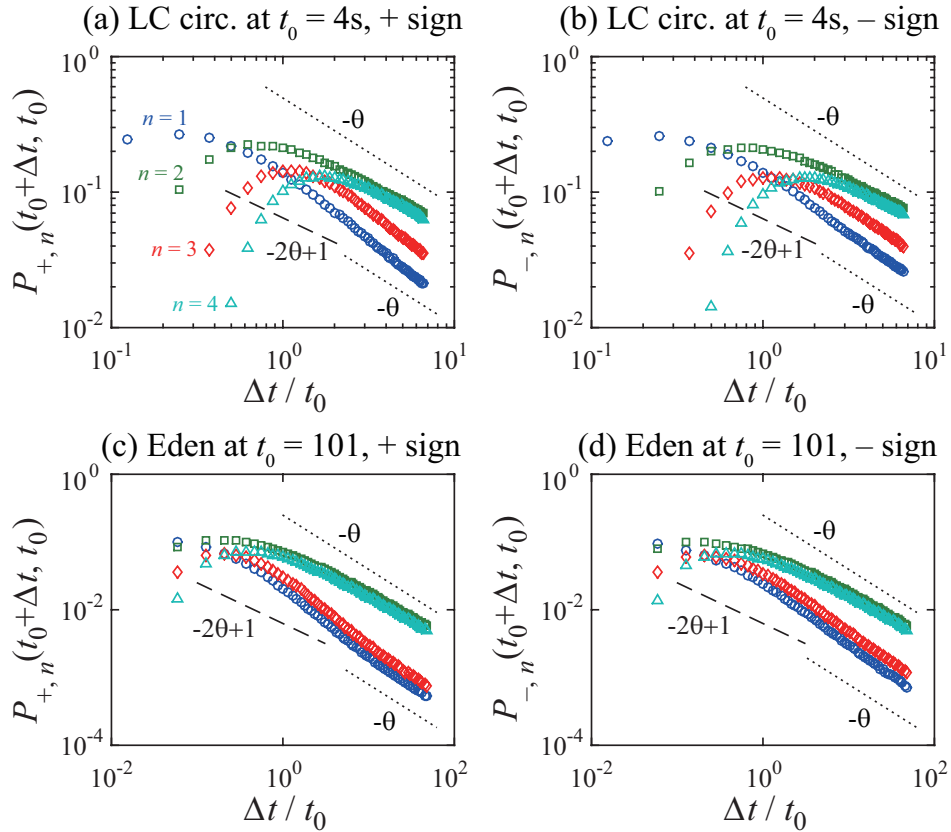


**Fig. 4** Generalized persistence probabilities  $P_{\pm, n}(t_0 + \Delta t, t_0)$  of the circular interfaces, measured for the positive (a,c) and negative (b,d) fluctuations (sign at  $t_0$  is used) in the LC experiment (a,b) and the Eden model (c,d). The dashed and dotted lines indicate exponents  $-2\theta + 1 = -0.6$  and  $-\theta = -0.8$ , respectively. The same set of colors/symbols and  $n$  is used in all panels.

decay than that of RP (after the initial growth, which occurs at  $\Delta t \lesssim n^{1/\theta} \tau_0$  for RP; see Appendix B). In other words,  $P_{\pm, n}(t_0 + \Delta t, t_0)$  has heavier weight in the short-time regime for odd  $n$ . This difference from RP gives nontrivial contribution to the sum in Eq. (8), which is absent for RP. We consider that this is how the different behavior of the correlation function arises, which captures, for KPZ, the characteristic time correlation of the (non-binarized) KPZ-class fluctuations.

### 3.2 Flat interfaces

Now we turn our attention to the flat interfaces. Figure 5 shows the waiting-time distribution (ccdf)  $p_{\pm}(\tau; t)$  for the flat LC experiment (main panels) and the dPNG model (insets). At short waiting times, we identify power-law decay with exponent  $-0.8$ . This exponent seems to be different from  $-2/3$  previously observed for a related quantity in the KPZ stationary state [25]<sup>5</sup>, but is identical to the one we found for the circular interfaces (Fig. 1). For the flat interfaces (Fig. 5), however, this power law is followed by another one with larger (in magnitude) exponent for longer waiting times, which now takes different values between positive and negative fluctuations. The measured exponents do not seem to reach their asymptotic values within our observation time, increasing gradually with  $\tau$ , but they are clearly asymmetric with respect to the sign, in sharp contrast with the exponent for the shorter waiting times or for the circular interfaces. Moreover,  $p_{\pm}(\tau; t)$  taken at different  $t$  overlaps when it is plotted against  $\tau/t$  (Fig. 5). This indicates that the value of  $\tau$  separating the

<sup>5</sup> The exponent measured in [25] was about the persistence probability of the sign of  $\Delta h(x, t) - \Delta h(x, t_0)$  with  $\Delta h(x, t) = h(x, t) - \int_0^L h(x, t) dx / L$ , whereas we measure here the waiting-time distribution, or the persistence probability of the sign of  $\delta h(x, t) = h(x, t) - \langle h(x, t) \rangle$  with the condition  $\delta h(x, t_0) = 0$ . Although both probabilities concern the first return to zero, the different definitions may lead to different exponent values.

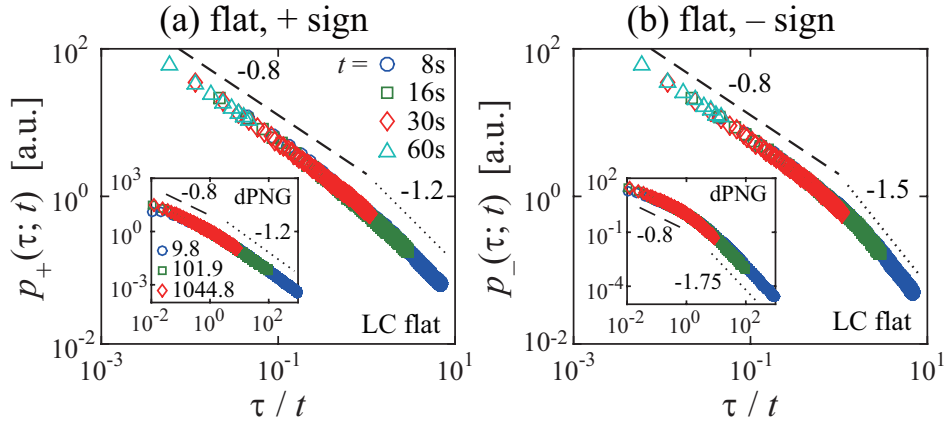


**Fig. 5** Waiting-time distributions (ccdfs)  $p_{\pm}(\tau;t)$  against  $\tau/t$  for the flat interfaces, obtained at different  $t$  in the LC experiment (main panels) and the dPNG model (insets). The dashed and dotted lines are guides to the eyes, indicating exponents labeled alongside, though for the dotted lines we expect larger asymptotic exponents (see text). The same set of colors/symbols and  $t$  is used in both panels. The ordinates are arbitrarily shifted.

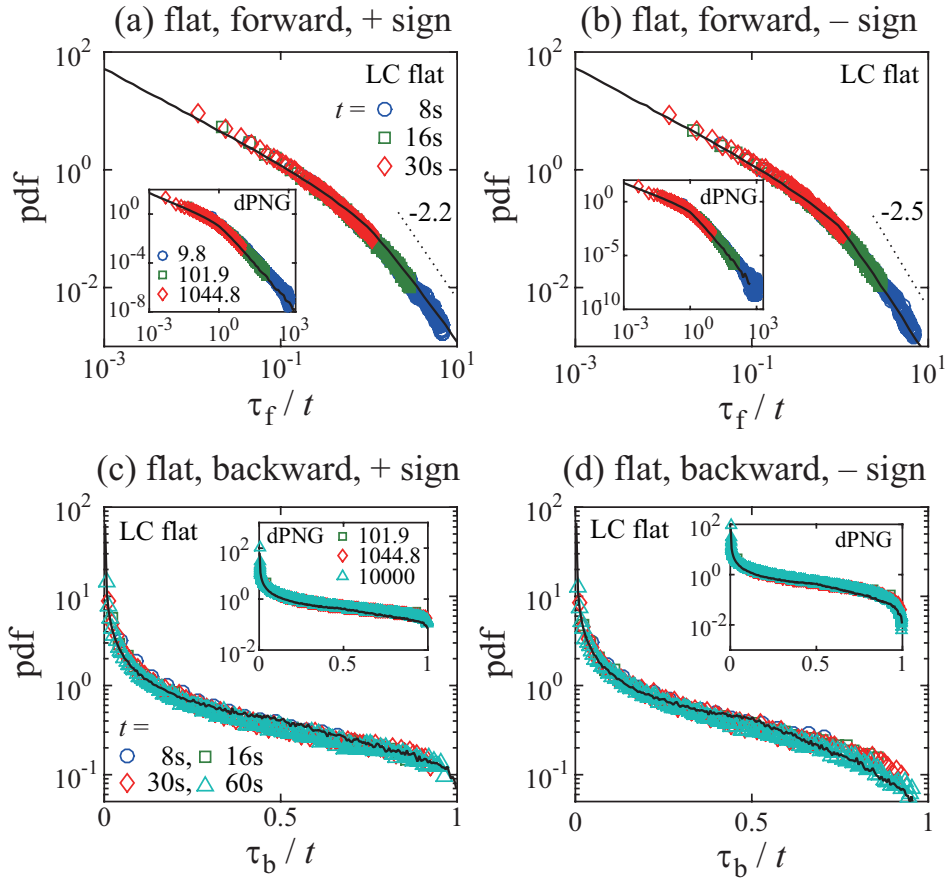


**Fig. 6** Distributions (pdfs) of the forward (a,b) and backward (c,d) recurrence times,  $\tau_f$  and  $\tau_b$ , respectively, for the flat interfaces at different  $t$  in the LC experiment (main panels) and the dPNG model (insets).  $\tau_f$  and  $\tau_b$  are rescaled by  $t$ . The black lines indicate numerical results for the 2-step RP at  $t = 10^7$ . The data are normalized so that they have the same statistical weight in the range covered by their abscissa. The same colors/symbols correspond to the same  $t$  in all panels.

two power-law regimes is not constant, but grows with  $t$ , showing the aging property of the waiting-time distribution.

These results on the flat-KPZ waiting-time distribution lead us to introduce a variant of RP with two power-law regimes, called hereafter the 2-step RP model <sup>6</sup>:

$$p_{\pm}(\tau; t) = \begin{cases} \left(\frac{\tau}{\tau_0}\right)^{-\theta} & \text{for } \tau_0 \leq \tau \leq t, \\ \left(\frac{t}{\tau_0}\right)^{-\theta} \left(\frac{\tau}{t}\right)^{-\theta'_{\pm}} & \text{for } t \leq \tau. \end{cases} \quad (10)$$

We then solved it numerically with  $\theta = 0.8$ ,  $\theta'_+ = 1.2$ ,  $\theta'_- = 1.5$  (as observed experimentally) in the following way: First, the initial sign was chosen to be either + or - with the equal probability. The first waiting time was generated according to  $p_{\pm}(\tau; t) = (\tau/\tau_0)^{-\theta'_{\pm}}$  ( $\tau \geq \tau_0$ ), because Eq. (10) is invalid for  $t = 0$ . Subsequent waiting times were generated by Eq. (10), until the time (cumulative sum of waiting times) exceeds the recording time  $T_{\text{tot}}$ . We sampled  $10^6$  independent realizations to investigate statistical properties of this 2-step RP model.

Now we compare this 2-step RP model and the flat KPZ interfaces. Figure 6 shows the forward and backward recurrence-time distributions. We find that these quantities for the flat KPZ interfaces are reproduced by the 2-step RP model reasonably well, similarly to those for the circular interfaces found in agreement with the standard RP. Aging of the recurrence-time distributions is also clear in both cases. Note however that, while  $\text{pdf}(\tau_f) \sim \tau_f^{-\theta}$  is known to hold for the standard RP [Eq. (4)] with  $1 < \theta < 2$  [18], our 2-step RP rather indicates  $\text{pdf}(\tau_f) \sim \tau_f^{-\theta'_{\pm}-1}$  [dotted lines in Fig. 6(a,b)]. Since  $\text{pdf}(\tau_f)$  is given by the derivative of the persistence probability, this implies  $\theta'_{\pm} = \theta_{\pm}^{(p)}$ , hence asymptotically  $\theta'_+ = 1.35$  and  $\theta'_- = 1.85$  are expected for the flat KPZ subclass.

In contrast to this agreement in the recurrence-time distributions, the distribution of the time-averaged sign  $\bar{\sigma} = (1/T) \int_0^T \sigma(x, t) dt$  turns out to be different between the flat KPZ subclass and the 2-step RP [Fig. 7(a)], analogously to the results for the circular interfaces. More specifically, both the flat KPZ subclass and the 2-step RP are found to show asymptotic broad distributions [Fig. 7(a)], hence both of them exhibit WEB, but the distributions are again clearly different between the two systems. Note here that the time-averaged sign distribution for the standard RP [Eq. (4)] with  $\theta > 1$  becomes infinitely narrow in the limit  $t \rightarrow \infty$  [18]; this is however not the case here, despite  $\theta'_{\pm} > 1$ . The existence of the broad distribution results from the aging of the waiting-time distribution, i.e., from the fact that the crossover time in the waiting-time distribution grows with  $t$  [see Fig. 5 and Eq. (10)].

The difference between the flat KPZ subclass and the 2-step RP is also detected in the correlation function of sign,  $C_{\text{sign}}(t, t_0) = \langle \sigma(x, t) \sigma(x, t_0) \rangle$ : while our simulations of the 2-step RP show  $C_{\text{sign}}(t, t_0) \sim t^{-\theta'_+}$  [Fig. 7(b)], for the flat interfaces it decays as  $t^{-\bar{\lambda}}$  with  $\bar{\lambda} = 1$  [Fig. 7(c,d)], the characteristic exponent for the decorrelation of the flat KPZ subclass [see Eq. (2)]. Similarly to the circular case, this difference results from correlation of waiting times, which can be characterized by the generalized persistence probability  $P_{\pm, n}(t_0 + \Delta t, t_0)$ . For the 2-step RP, i.e., in the absence of correlation, we numerically find [Fig. 8(a,b)]

$$P_{\pm, n \geq 1}(t_0 + \Delta t, t_0) \sim \begin{cases} \Delta t^{-2\theta+1} & \text{for } \Delta t \ll t_0, \\ \Delta t^{-\theta'_{\pm}} & \text{for } \Delta t \gg t_0, \end{cases} \quad (11)$$

where in the latter case the two double signs are set to be the same sign for even  $n$  and the opposite ones for odd  $n$ . This long-time behavior can also be seen in the flat KPZ subclass [Fig. 8(c,d) for the LC experiment and (e,f) for the dPNG model]. In contrast, short-time behavior of  $P_{\pm, n \geq 1}$  is found to be different between the 2-step RP and the flat KPZ subclass [compare data and the dashed lines in Fig. 8(c-f)], the latter carrying heavier weight in the short-time regime. Analogously to the circular case, such pronounced short-time behavior of  $P_{\pm, n \geq 1}$  seems to generate, via Eq. (8), the characteristic decay of the correlation function  $C_{\text{sign}}(t, t_0)$  slower than that of the 2-step RP [Fig. 7(b)].

<sup>6</sup> Strictly, since the evolution of the 2-step RP model [Eq. (10)] depends on  $t$ , it is *not* in the scope of the models considered in the renewal theory.



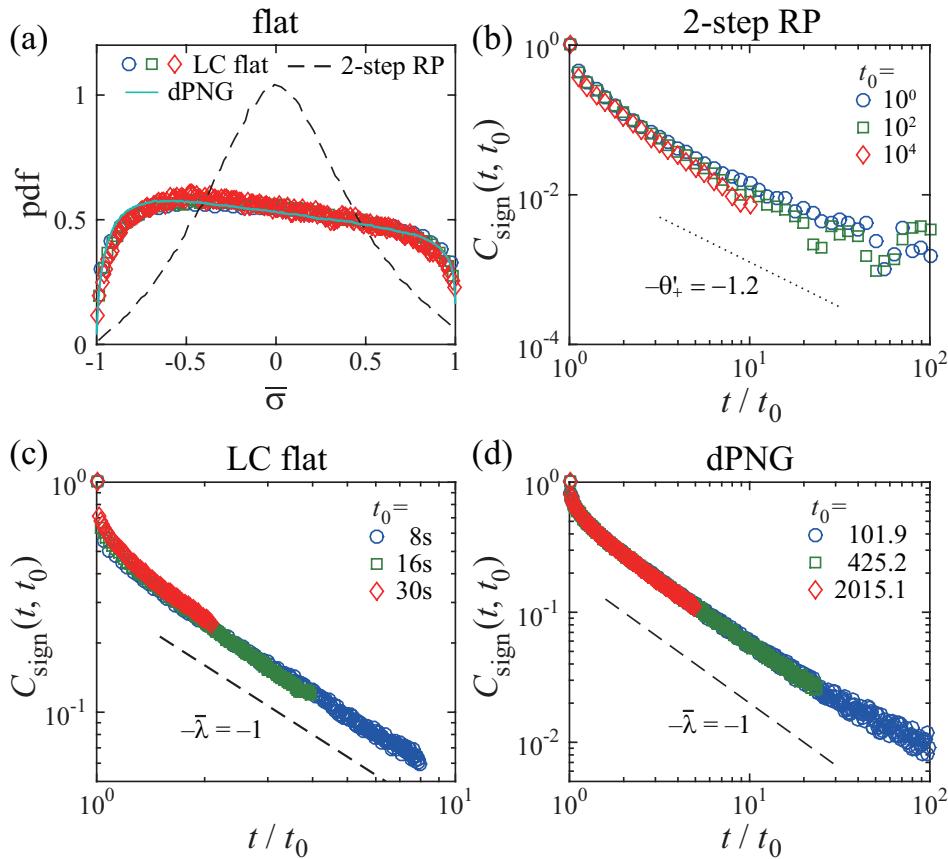


**Fig. 7** Time-averaged sign distribution (a) and sign correlation function (b-d) for the flat interfaces (a,c,d) and the 2-step RP (b). (a) Pdf of the time-averaged sign  $\bar{\sigma} = (1/T) \int_0^T \sigma(x,t) dt$  for the LC experiment ( $T = 15$  s, 30 s, 63 s for circles, squares, and diamonds, respectively) and the dPNG model ( $T = 10000$ ; turquoise line), compared to numerical data for the 2-step RP ( $T = 10^7$ ; dashed line). The gray vertical line indicates the ensemble-averaged value  $\langle \bar{\sigma} \rangle = -0.0316$ . The existence of the broad asymptotic distribution is a direct evidence of WEB in the flat KPZ subclass, but in the form different from that of the circular case. (b-d) Correlation function of sign,  $C_{\text{sign}}(t, t_0) = \langle \sigma(x,t) \sigma(x, t_0) \rangle$ , at different  $t_0$  for the 2-step RP ( $T_{\text{tot}} = 10^6$ ) (b), the LC flat interfaces (c), and the dPNG model (d). The dashed lines in the panels (c,d) indicate the exponent  $-\bar{\lambda} = -1$ , while the dotted line in the panel (b) shows  $-\theta'_+ = -1.2$ .

#### 4 Concluding remarks

We have shown an unexpected similarity between sign renewals of the KPZ-class fluctuations and RP, studied in the context of aging phenomena and WEB. Despite the fundamental difference between the two systems, we found, for the circular interfaces, that the KPZ waiting times obey simple power-law distributions identical to those defining RP, while those for the flat interfaces correspond to its straightforward extension with two power-law regimes [Eq. (10), the 2-step RP model]. Further quantitative agreement has been found in the recurrence-time distributions (Figs. 2 and 6), from which the agreement in the persistence probability follows. These quantities have remained theoretically intractable for KPZ, but now, following the agreement we found, their precise forms are revealed for the circular interfaces, thanks to the exact solutions for the original RP. This also implies that recurrence-time statistics may be determined independently of the intercorrelation of waiting times, contrary to the usual beliefs.

The correlated waiting times of KPZ otherwise generate characteristic aging properties of the KPZ-class fluctuations (Figs. 3 and 7), especially their broad asymptotic distributions of the time-averaged sign. This indicates WEB of the KPZ-class fluctuations, which turned out to be different from that of RP, and in fact also from other types of WEB, known from the studies of single-particle observations. We therefore consider that the WEB found in this study is of a new kind, characteristic of many-body problems governed by the

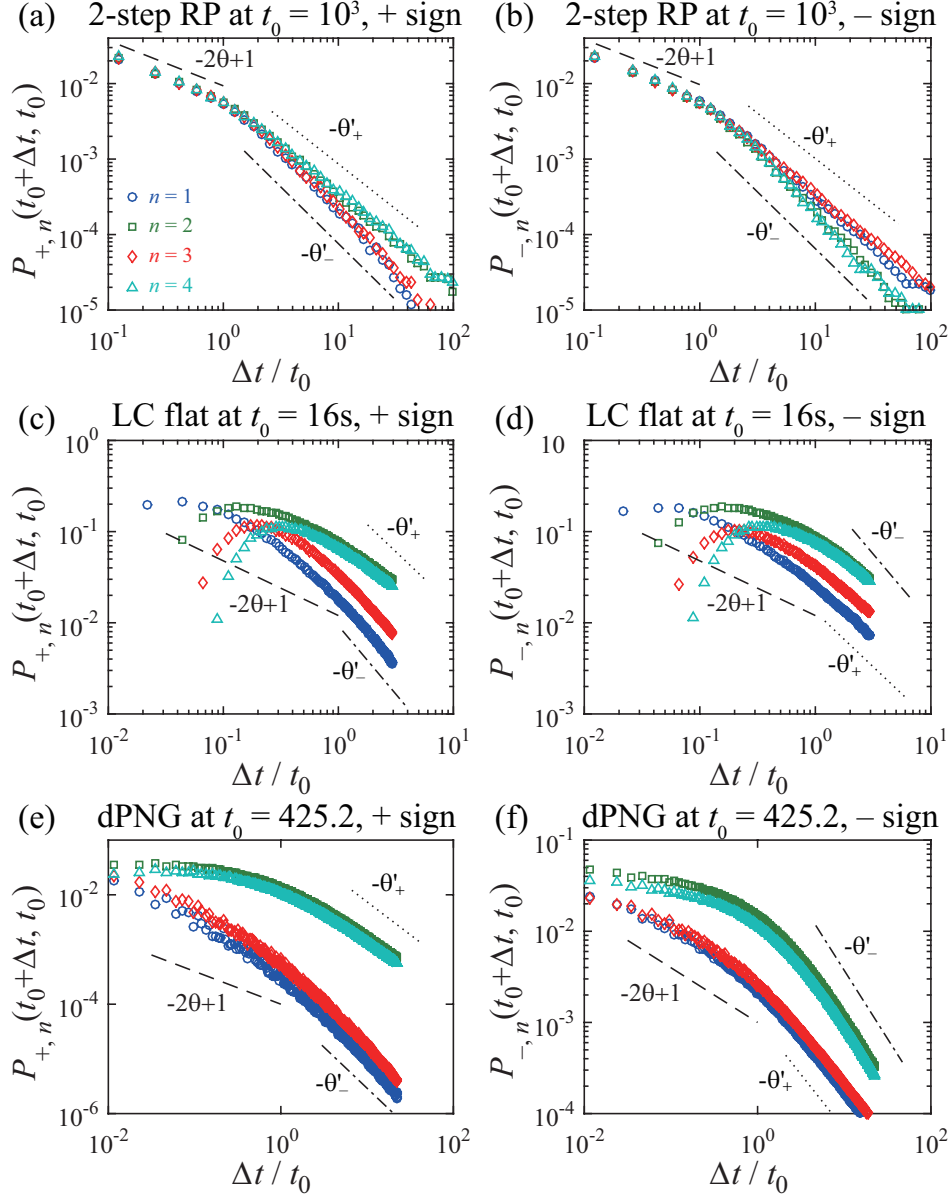


**Fig. 8** Generalized persistence probabilities  $P_{\pm, n}(t, t_0)$  for the 2-step RP ( $T_{\text{tot}} = 10^6$ ) (a,b) and for the flat KPZ-class interfaces [LC experiment (c,d) and dPNG model (e,f)], measured for the positive (a,c,e) and negative (b,d,f) signs. The dashed lines in all panels indicate the exponent  $-2\theta + 1 = -0.6$  found in the short-time regime ( $\Delta t \ll t_0$ ) of the 2-step RP. The dotted and dot-dashed lines are guides for the eyes indicating exponents  $-\theta'_+$  and  $-\theta'_-$ , respectively, which characterize the long-time regime for the 2-step RP [see Eq. (11)]. The same set of colors/symbols and  $n$  is used in all panels.

KPZ universality class. This also implies that RP cannot be a proxy for the full KPZ dynamics; instead RP reproduces only some of the time-correlation properties of KPZ, surprisingly well, though.

In fact, such a partial similarity to RP was also argued in the past for the fractional Brownian motion (FBM), in the context of linear growth processes. Krug *et al.* [28] showed, for the stationary state of linear growth processes, that the stochastic process  $h(x, t) - h(x, t_0)$  is equivalent to FBM. Its first-return time (corresponding to the waiting time of its sign) is then characterized by a power-law distribution with exponent  $\theta = 1 - \beta$  [19, 10, 28] with  $\beta$  being the growth exponent, or the Hurst exponent of FBM. Cakir *et al.* [6] then suggested that the sign of FBM would form RP, showing numerical observations of its persistence probability as a partial support, but it turned out later that the two models behave differently in other statistical quantities

[17], because of the intercorrelation of waiting times. In our contribution, we studied the growth regime of nonlinear growth processes in the KPZ class and compared the sign of the stochastic process  $h(x,t) - \langle h(x,t) \rangle$  with RP. As already summarized, we showed thereby precise agreement in the waiting-time distribution and the persistence probability, but not in the other statistical properties we studied. Understanding the mechanism of this partial agreement is an important issue left for future studies, all the more because no theoretical understanding has been made so far on persistence properties of the KPZ growth regime [4]. Such developments will also help to understand the deviations from RP, which we believe carry characteristic information of underlying growth processes (recall our results on the correlation function). We hope this direction of analysis may afford a clue to elucidate hitherto unexplained time-correlation properties of the KPZ class. We also believe that our approach may be useful to characterize other scale-invariant processes such as critical phenomena.

**Acknowledgements** We acknowledge fruitful discussions with E. Barkai, I. Dornic, C. Godrèche, and S. N. Majumdar. This work is supported in part by KAKENHI from JSPS (No. JP25707033 and No. JP25103004), the JSPS Core-to-Core Program “Non-equilibrium dynamics of soft matter and information”, and the National Science Foundation under Grant No. NSF PHY11-25915.

## Appendix A Studied systems

In this appendix we briefly describe the three systems studied in this paper, namely the LC experiment [49,48], the off-lattice Eden model [45], and the dPNG model, all known to be in the KPZ class. The experimental results are obtained from the raw data acquired in Refs. [49,48]. The readers are referred to these publications for the complete description of the experimental system.

### Appendix A.1 LC experiment

The experiment concerns fluctuating interfaces between two turbulent regimes of electrically driven nematic liquid crystal, called the dynamic scattering modes 1 and 2 (DSM1 and DSM2, respectively) [47,49,48]. The DSM1/DSM2 configuration can be argued to lie in pure two dimensions<sup>7</sup>, so the interfaces in between are one-dimensional. Under sufficiently high applied voltage, here 26 V, DSM2 is more stable than DSM1, and the interfaces grow until the whole system is occupied by DSM2. The initial nucleus of the DSM2 state can be introduced by shooting laser pulses. This allows us to study both circular and flat growing interfaces: circular interfaces grow from a point nucleus generated by focused laser pulses, while flat interfaces originate from a linear region of DSM2, created by linearly expanded laser pulses.

In Refs. [49,48], Takeuchi and Sano measured 955 circular interfaces over time length 30.5 s and 1128 flat interfaces over 63 s, and found the characteristic statistical properties of the circular and flat KPZ subclasses, respectively. In the present study, we employ the same data sets which are guaranteed to belong to these subclasses, and analyze the sign of the height fluctuations as explained in the main text. The sign renewals are detected at every 0.5 s and 0.35 s for the circular and flat interfaces, respectively.

### Appendix A.2 Off-lattice Eden model

Numerical data for circular interfaces are obtained with the off-lattice Eden model, the version introduced in Ref. [45] which is sometimes called the off-lattice Eden D model. While detailed descriptions can be found in Ref. [45], in this model, one starts with a round particle of unit diameter placed at the origin of two-dimensional continuous space. At each time step, one randomly chooses one of the  $N$  existing particles, and attempts to put an identical particle next to it in a direction randomly chosen from the range  $[0, 2\pi)$ . If the new particle does not overlap any existing particles, it is added as attempted, otherwise the particle is discarded. Time  $t$  is then increased by  $1/N$ , whether the attempt is adopted or not. Particles without enough adjacent space, to which no particle can be added any more, are labelled inactive and excluded from the particle counter  $N$  (but can still block new particles). Since we are interested in the interface, or specifically the outermost closed loop of adjacent particles, particles surrounded by the interface are also marked inactive and treated likewise. This model was previously shown to belong to the circular KPZ subclass [45]. The data presented in the present paper are newly obtained from 5000 independent simulations of time length 5000, and the sign renewals are detected at every time unit.

---

<sup>7</sup> This is because the DSM2 state, known to consist of densely entangled topological defects, needs to break surface anchoring on the bottom and top plates to be sustained in the system.

### Appendix A.3 dPNG model

Numerical simulations of flat interfaces are performed with the dPNG model. This is a discretized version of the PNG model, which is one of the exactly solvable models in the  $(1+1)$ -dimensional KPZ class [37]. The evolution of the height variable  $h(x = i\Delta x, t = n\Delta t)$  of the dPNG model, with non-negative integers  $h, i, n$ , is given by the following equation:

$$h(x, t + \Delta t) = \max\{h(x - \Delta x, t), h(x, t), h(x + \Delta x, t)\} + \eta(x, t), \quad (12)$$

where  $\eta(x, t)$  is an independent and identically distributed random variable generated from the geometric distribution,  $\text{Prob}(\eta = k) = (1-p)^k p$  with  $p = \rho \Delta x \Delta t$ . The original PNG model with nucleation rate  $\rho$  and nucleus expansion rate  $\Delta x / \Delta t$  is retrieved by the continuum limit  $\Delta x \rightarrow 0$  and  $\Delta t \rightarrow 0$ .

In our study, we set  $\rho = 2, \Delta x = \Delta t = 0.1$  and the periodic boundary condition  $h(L, t) = h(0, t)$  with  $L = 10^4$  (or  $10^5$  lattice units). We start from the flat initial condition  $h(x, 0) = 0$  and evolve the system until  $t = 10^4$  by  $10^4$  independent simulations. The sign renewals are detected at every time step, i.e.,  $\Delta t = 0.1$  time unit. Note that the dPNG model with  $\Delta x = \Delta t = 0.1$  shows the same universal statistical properties as the original PNG model, provided that the height variable  $h(x, t)$  is appropriately rescaled using non-universal scaling coefficients [ $v_\infty$  and  $\Gamma$  in Eq. (1)]. The values of the scaling coefficients depend on  $\Delta x$  and  $\Delta t$ : for example, they are estimated at  $v_\infty \approx 2.2408$  and  $\Gamma \approx 1.571$  for the dPNG model studied here (the evaluation method described in Ref. [48] is used), while the values for the original PNG model (corresponding to  $\Delta x, \Delta t \rightarrow 0$ ) are  $v_\infty = 2$  and  $\Gamma = 1$ .

### Appendix B Generalized persistence probability for RP

Here we derive two asymptotic behaviors of the generalized persistence probability for the renewal process with a power-law waiting-time distribution. We assume Eq. (4) with  $\theta < 1$  for the waiting time distribution. Thus, the Laplace transform of the probability density function (pdf) of waiting times  $\tau$ ,  $\hat{\rho}(\tau) \equiv p'(\tau)$ , is given by

$$\hat{\rho}(s) = 1 - as^\theta + \mathcal{O}(s), \quad (13)$$

with  $a = \Gamma(1-\theta)\tau_0^\theta$  [18]. The generalized persistent probability can be represented by

$$P_n(t_0 + \Delta t, t_0) = \text{Prob}[\Delta t_n < \Delta t; t_0] - \text{Prob}[\Delta t_{n+1} < \Delta t; t_0], \quad (14)$$

where  $\text{Prob}[\Delta t_n < \Delta t; t_0]$  is the probability that  $\Delta t_n \equiv \tau_f(t_0) + \tau_2 + \dots + \tau_n < \Delta t$  holds, with waiting times  $\tau_i$  and the forward recurrence time  $\tau_f(t_0)$  (time elapsed from  $t_0$  to the first renewal event since then). For  $n \geq 1$ , the double Laplace transform of  $P_n(t_0 + \Delta t, t_0)$  with respect to  $t_0$  and  $\Delta t$  can be calculated as follows:

$$\begin{aligned} \hat{P}_n(s, u) &\equiv \int_0^\infty \int_0^\infty P_n(t_0 + \Delta t, t_0) e^{-st_0 - u\Delta t} dt_0 d\Delta t \\ &= \frac{\hat{f}_E(u; s) \hat{\rho}(u)^{n-1}}{u} - \frac{\hat{f}_E(u; s) \hat{\rho}(u)^n}{u}, \end{aligned} \quad (15)$$

where  $\hat{f}_E(u; s)$  is the double Laplace transform of  $\text{pdf}(\tau_f(t_0); t_0)$ , given by [18]

$$\begin{aligned} \hat{f}_E(u; s) &\equiv \int_0^\infty \int_0^\infty \text{pdf}(\tau_f; t_0) e^{-u\tau_f - st_0} d\tau_f dt_0 \\ &= \frac{\hat{\rho}(u) - \hat{\rho}(s)}{s - u} \frac{1}{1 - \hat{\rho}(s)}. \end{aligned} \quad (16)$$

Therefore,

$$\hat{P}_n(s, u) = \frac{\hat{\rho}(u) - \hat{\rho}(s)}{s - u} \frac{1}{1 - \hat{\rho}(s)} \hat{\rho}(u)^{n-1} \frac{1 - \hat{\rho}(u)}{u}. \quad (17)$$

Now we consider the following two asymptotic limits. For  $u \ll s \ll \tau_0^{-1}$  ( $\tau_0 \ll t_0 \ll \Delta t$ ), we obtain

$$\hat{P}_n(s, u) \simeq \frac{1}{s} au^{\theta-1}, \quad (18)$$

where we used approximation  $\hat{\rho}(u)^{n-1} \simeq 1 - a(n-1)u^\theta \simeq 1$ . In other words,  $u$  is so small that  $a(n-1)u^\theta \ll 1$ , i.e.,  $\Delta t \gg (n-1)^{1/\theta} \tau_0 \simeq n^{1/\theta} \tau_0$ . Then the inverse Laplace transform yields

$$P_n(t_0 + \Delta t, t_0) \simeq \left( \frac{\Delta t}{\tau_0} \right)^{-\theta}, \quad (19)$$

for  $\tau_0 \ll t_0 \ll \Delta t$  and  $\Delta t \gg n^{1/\theta} \tau_0$ . We note that this asymptotic behavior does not depend on  $t_0$  nor  $n$ . In contrast, for  $s \ll u \ll \tau_0^{-1}$  ( $\tau_0 \ll \Delta t \ll t_0$ ),

$$\hat{P}_n(s, u) \simeq \frac{1}{s^\theta} au^{2\theta-2}, \quad (20)$$

where we used the same approximation as in the previous case. The inverse Laplace transform then yields

$$P_n(t_0 + \Delta t, t_0) \simeq \frac{\Gamma(1-\theta)}{\Gamma(\theta)\Gamma(2-2\theta)} \left(\frac{t_0}{\tau_0}\right)^{-1+\theta} \left(\frac{\Delta t}{\tau_0}\right)^{-2\theta+1}, \quad (21)$$

for  $n^{1/\theta}\tau_0 \ll \Delta t \ll t_0$ . This asymptotic behavior is independent of  $n$  but does depend on  $t_0$ .

## References

1. Akimoto, T., Miyaguchi, T.: Distributional ergodicity in stored-energy-driven lévy flights. *Phys. Rev. E* **87**, 062,134 (2013)
2. Barabási, A.L., Stanley, H.E.: *Fractal Concepts in Surface Growth*. Cambridge Univ. Press, Cambridge (1995)
3. Bouchaud, J.P.: Weak ergodicity breaking and aging in disordered systems. *J. Phys. I (France)* **2**, 1705–1713 (1992)
4. Bray, A.J., Majumdar, S.N., Schehr, G.: Persistence and first-passage properties in nonequilibrium systems. *Adv. Phys.* **62**, 225–361 (2013)
5. Brokmann, X., Hermier, J.P., Messin, G., Desbrières, P., Bouchaud, J.P., Dahan, M.: Statistical aging and nonergodicity in the fluorescence of single nanocrystals. *Phys. Rev. Lett.* **90**, 120,601 (2003)
6. Cakir, R., Grigolini, P., Krokhin, A.A.: Dynamical origin of memory and renewal. *Phys. Rev. E* **74**, 021,108 (2006)
7. Carrasco, I.S.S., Takeuchi, K.A., Ferreira, S.C., Oliveira, T.J.: Interface fluctuations for deposition on enlarging flat substrates. *New J. Phys.* **16**, 123,057 (2014)
8. Corwin, I.: The Kardar-Parisi-Zhang equation and universality class. *Random Matrices Theory Appl.* **1**, 1130,001 (2012)
9. Cox, D.R.: *Renewal Theory*. Methuen, London (1962)
10. Ding, M., Yang, W.: Distribution of the first return time in fractional brownian motion and its application to the study of on-off intermittency. *Phys. Rev. E* **52**, 207–213 (1995)
11. Dornic, I., Godrèche, C.: Large deviations and nontrivial exponents in coarsening systems. *J. Phys. A* **31**, 5413–5429 (1998)
12. Dotsenko, V.: Two-time free energy distribution function in (1+1) directed polymers. *J. Stat. Mech.* **2013**, P06,017 (2013)
13. Dotsenko, V.: Two-time free energy distribution function in the kpz problem. arXiv:1507.06135 (2015)
14. Dynkin, E.B.: Some limit theorems for sums of independent random variables with infinite mathematical expectations. *Izv. Akad. Nauk SSSR Ser. Mat.* **19**, 247–266 (1955). Selected Translations Math. Stat. Prob **1**, 171–189 (1961).
15. Feller, W.: *An Introduction to Probability Theory and Its Applications*, vol. 1, 3 edn. Wiley, New York (1968)
16. Ferrari, P.L., Spohn, H.: On the current time correlations for one-dimensional exclusion processes. arXiv:1602.00486 (2016)
17. García-García, R., Rosso, A., Schehr, G.: Longest excursion of fractional brownian motion: Numerical evidence of non-markovian effects. *Phys. Rev. E* **81**, 010,102 (2010)
18. Godrèche, C., Luck, J.M.: Statistics of the occupation time of renewal processes. *J. Stat. Phys.* **104**, 489–524 (2001)
19. Hansen, A., Engøy, T., Måløy, K.J.: Measuring hurst exponents with the first return method. *Fractals* **02**(04), 527–533 (1994)
20. He, Y., Burov, S., Metzler, R., Barkai, E.: Random time-scale invariant diffusion and transport coefficients. *Phys. Rev. Lett.* **101**, 058,101 (2008)
21. Hérault, J., Pétrélis, F., Fauve, S.:  $1/f^\alpha$  low frequency fluctuations in turbulent flows. *J. Stat. Phys.* **161**, 1379–1389 (2015)
22. Hérault, J., Pétrélis, F., Fauve, S.: Experimental observation of  $1/f$  noise in quasi-bidimensional turbulent flows. *Europhys. Lett.* **111**, 44,002 (2015)
23. Jeon, J.H., Tejedor, V., Burov, S., Barkai, E., Selhuber-Unkel, C., Berg-Sørensen, K., Oddershede, L., Metzler, R.: *In Vivo* anomalous diffusion and weak ergodicity breaking of lipid granules. *Phys. Rev. Lett.* **106**, 048,103 (2011)
24. Johansson, K.: Two time distribution in brownian directed percolation. arXiv:1502.00941 (2015)
25. Kallabis, H., Krug, J.: Persistence of Kardar-Parisi-Zhang interfaces. *Europhys. Lett.* **45**, 20–25 (1999)
26. Kardar, M., Parisi, G., Zhang, Y.C.: Dynamic scaling of growing interfaces. *Phys. Rev. Lett.* **56**, 889–892 (1986)
27. Kriecherbauer, T., Krug, J.: A pedestrian’s view on interacting particle systems, kpz universality and random matrices. *J. Phys. A* **43**, 403,001 (2010)
28. Krug, J., Kallabis, H., Majumdar, S.N., Cornell, S.J., Bray, A.J., Sire, C.: Persistence exponents for fluctuating interfaces. *Phys. Rev. E* **56**, 2702–2712 (1997)
29. Kuno, M., Fromm, D.P., Hamann, H.F., Gallagher, A., Nesbitt, D.J.: Nonexponential “blinking” kinetics of single cdse quantum dots: A universal power law behavior. *J. Chem. Phys.* **112**, 3117 (2000)
30. Lamperti, J.: An occupation time theorem for a class of stochastic processes. *Trans. Amer. Math. Soc.* **88**, 380–387 (1958)
31. Manzo, C., Torreno-Pina, J.A., Massignan, P., Lapeyre, G.J., Lewenstein, M., Garcia Parajo, M.F.: Weak ergodicity breaking of receptor motion in living cells stemming from random diffusivity. *Phys. Rev. X* **5**, 011,021 (2015)
32. Margolin, G., Barkai, E.: Nonergodicity of blinking nanocrystals and other lévy-walk processes. *Phys. Rev. Lett.* **94**, 080,601 (2005)
33. Margolin, G., Barkai, E.: Nonergodicity of a time series obeying lévy statistics. *J. Stat. Phys.* **122**, 137–167 (2006)
34. Metzler, R., Jeon, J.H., Cherstvy, A.G., Barkai, E.: Anomalous diffusion models and their properties: non-stationarity, non-ergodicity, and ageing at the centenary of single particle tracking. *Phys. Chem. Chem. Phys.* **16**, 24,128–24,164 (2014)
35. Miyaguchi, T., Akimoto, T.: Intrinsic randomness of transport coefficient in subdiffusion with static disorder. *Phys. Rev. E* **83**, 031,926 (2011)
36. Miyaguchi, T., Akimoto, T.: Anomalous diffusion in a quenched-trap model on fractal lattices. *Phys. Rev. E* **91**, 010,102 (2015)
37. Prähofer, M., Spohn, H.: Universal distributions for growth processes in 1 + 1 dimensions and random matrices. *Phys. Rev. Lett.* **84**, 4882–4885 (2000)
38. Schulz, J.H.P., Barkai, E., Metzler, R.: Aging effects and population splitting in single-particle trajectory averages. *Phys. Rev. Lett.* **110**, 020,602 (2013)

- 
39. Schulz, J.H.P., Barkai, E., Metzler, R.: Aging renewal theory and application to random walks. *Phys. Rev. X* **4**, 011,028 (2014)
  40. Singha, S.B.: Persistence of surface fluctuations in radially growing surfaces. *J. Stat. Mech.* **2005**, P08,006 (2005)
  41. Spohn, H.: Fluctuating hydrodynamics approach to equilibrium time correlations for anharmonic chains. arXiv:1505.05987 (2015)
  42. Stefani, F.D., Hoogenboom, J.P., Barkai, E.: Beyond quantum jumps: Blinking nanoscale light emitters. *Phys. Today* **62**, 34 (2009)
  43. Stefani, F.D., Zhong, X., Knoll, W., Han, M., Kreiter, M.: Memory in quantum-dot photoluminescence blinking. *New J. Phys.* **7**, 197 (2005)
  44. Tabei, S.M.A., Burov, S., Kim, H.Y., Kuznetsov, A., Huynh, T., Jureller, J., Philipson, L.H., Dinner, A.R., Scherer, N.F.: Intracellular transport of insulin granules is a subordinated random walk. *Proc. Natl. Acad. Sci. USA* **110**(13), 4911–4916 (2013)
  45. Takeuchi, K.A.: Statistics of circular interface fluctuations in an off-lattice eden model. *J. Stat. Mech.* **2012**, P05,007 (2012)
  46. Takeuchi, K.A.: Experimental approaches to universal out-of-equilibrium scaling laws: turbulent liquid crystal and other developments. *J. Stat. Mech.* **2014**, P01,006 (2014)
  47. Takeuchi, K.A., Sano, M.: Universal fluctuations of growing interfaces: Evidence in turbulent liquid crystals. *Phys. Rev. Lett.* **104**, 230,601 (2010)
  48. Takeuchi, K.A., Sano, M.: Evidence for geometry-dependent universal fluctuations of the kardar-parisi-zhang interfaces in liquid-crystal turbulence. *J. Stat. Phys.* **147**, 853–890 (2012)
  49. Takeuchi, K.A., Sano, M., Sasamoto, T., Spohn, H.: Growing interfaces uncover universal fluctuations behind scale invariance. *Sci. Rep.* **1**, 34 (2011)
  50. Weigel, A.V., Simon, B., Tamkun, M.M., Krapf, D.: Ergodic and nonergodic processes coexist in the plasma membrane as observed by single-molecule tracking. *Proc. Natl. Acad. Sci. USA* **108**, 6438–6443 (2011)
  51. Wong, I.Y., Gardel, M.L., Reichman, D.R., Weeks, E.R., Valentine, M.T., Bausch, A.R., Weitz, D.A.: Anomalous diffusion probes microstructure dynamics of entangled f-actin networks. *Phys. Rev. Lett.* **92**, 178,101 (2004)
  52. Yamamoto, E., Akimoto, T., Yasui, M., Yasuoka, K.: Origin of 1/f noise in hydration dynamics on lipid membrane surfaces. *Sci. Rep.* **5**, 8876 (2015)
  53. Yamamoto, E., Kalli, A.C., Akimoto, T., Yasuoka, K., Sansom, M.S.P.: Anomalous dynamics of a lipid recognition protein on a membrane surface. *Sci. Rep.* **5**, 18,245 (2015)

